23^{th} Annual Workshop on
Mathematical Problems in Industry
University of Delaware, June 11–15, 2007

Maximizing Minimum Pressure in Fluid Dynamic Bearings of Hard Disk Drives

Problem presented by
Ferdinand Hendriks
Hitachi GST

Participants:

Kara Maki (U-Delaware)	Alfa Heryudono (U-Delaware)
Melih Ozlem (RPI)	Kishor Bhalezcio (RPI)
Don Schwendeman (RPI)	Agegnehu Atena (U-Buffalo)
Colin Please (U-Southampton)	Tom Witelski (Duke)
Joel Phillips (McGill)	Jiguang Sun (Delaware State)
Michael Case (Clemson)	Joseph Fehribach (WPI)

Summary Presentation given by J. Phillips (6/15/07)
(August 31 2007, Version 4)

1 Introduction

Engineering design of computer hard disk drives is a continuously evolving area where fierce competition drives innovations in smaller, faster, higher-density designs. Different elements of the overall hard drive design involve various branches of science and engineering including materials science, electromagnetics, control theory, electrical engineering, mechanical engineering and fluid dynamics. The focus of our current work is the central spindle which supports the rotating magnetic platters which hold all of the data, see Fig. 1. The spindle must operate with great precision and stability at high rotational speeds. Design practice has converged on oil-lubricated hydrodynamic journal bearings as the most common choice for spindles. That is, a layer of viscous oil separates a rotating shaft (the bearing) from the fixed outer sleeve (the journal), see cross-section in Fig 1(right). In hard drives, it is very important for the shaft to be centered within the sleeve. Plain journal bearings (i.e. both surfaces are circular cylinders) are unstable to perturbations that push the shaft off-center. It was found that this stability problem can be overcome by cutting diagonal grooves into the journal in a pattern called a herring-bone, see Fig. 2 [4, 8, 13, 14, 17, 18]. Another consequence of this design is that very high pressures are generated by the grooves as they drive the oil to the middle of the bearing, away from the top/bottom ends of the spindle. This pumping action generally works to oppose leakage out of the bearing [8, 14, 17, 18].

In this report we examine how choices for the groove pattern can influence the key properties of the bearing. The focus is to understand the effect of the groove geometry on the pumping action. In particular the undesirable behavior caused by the low pressures created near the top/bottom ends of the bearing which, under many conditions, may result in the pressure becoming negative, relative to atmospheric pressure. Negative pressure can result in cavitation or, when it occurs near an air-oil interface, can cause air to be ingested and hence create bubbles. Any bubbles in the oil can corrupt the lubricating layer in the bearing [11, 16] and, as they are created and collapse, can cause significant undesirable vibrations. The negative pressures have therefore been identified

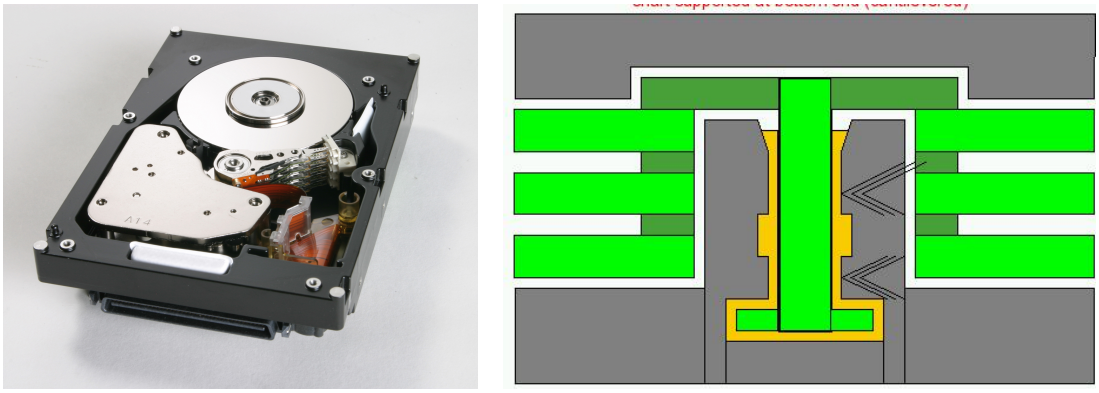

Figure 1: Left: A photograph of the mechanical elements in a modern hard disk drive, Right: A schematic of the cross-section of the spindle and platters. Note the oil (yellow) between the spindle's central shaft and circular sleeve walls.

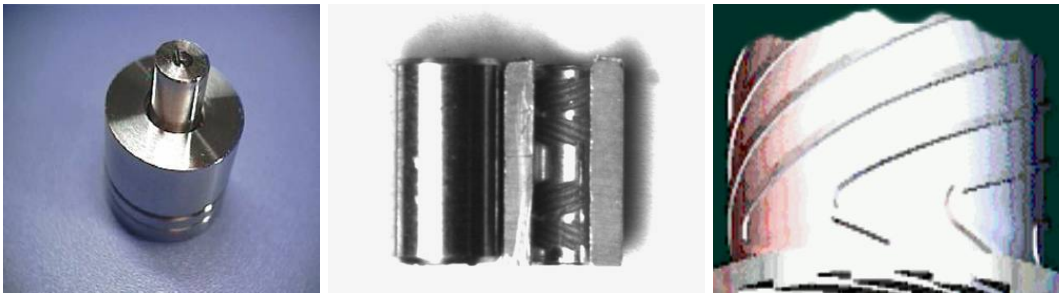

Figure 2: Herring-bone journal bearings, 3 views: (left) full assembly, (middle) cross-section of the journal showing the herring-bone grooves, and (right) a computer-generated image of herring-bone grooves on a bearing.

as one of the key problems in design of hard disk drive bearings [1, 2, 15]. We will use numerical computations and some analysis to show that by modifying the groove geometry we can reduce the negative pressure while retaining good stability characteristics.

2 Problem formulation

2.1 Geometric considerations and physical parameters

The analysis of the general problem for journal bearings can be quite involved but for our restricted goals, we can use geometric considerations to simplify the problem. The gap between the journal and the bearing (called the clearance) is very small compared to the radius of the journal, consequently curvature effects can be neglected and the cylindrical geometry can be "un-wrapped" to a rectangular form with the horizontal direction representing arclength around the journal, $\tilde{x} = \tilde{R}\theta$, where $\tilde{R}$ is the radius of the bearing, see Figure 3. We will consider journals with symmetric herring-bone

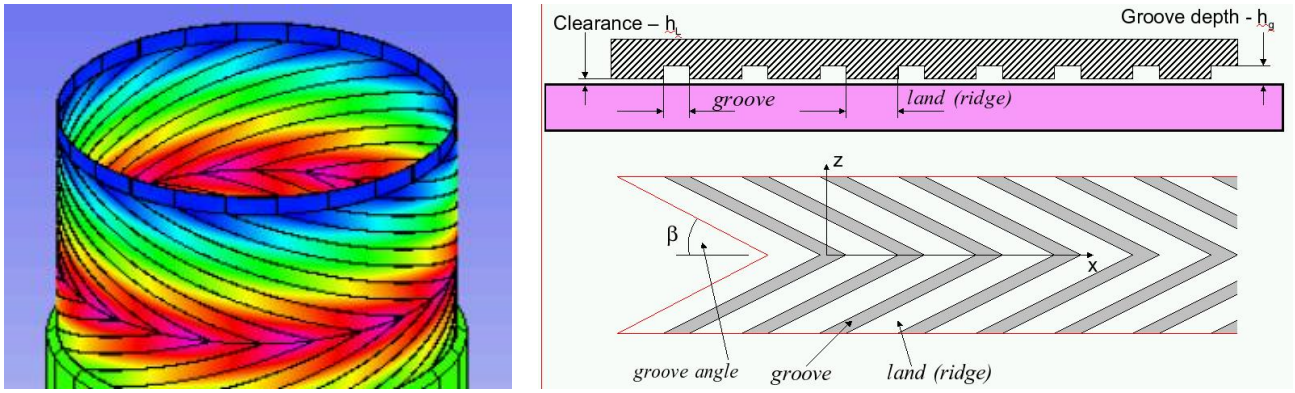

Figure 3: Unwrapping the cylindrical herring-bone bearing to a rectangular form: (left) physical configuration, (right) unwrapped representation.

patterns [17] and we label the half-height to be $\tilde{H}$. The angular velocity of the bearing taken to be a constant $\tilde{\Omega}$ which is on the order of 10,000 rpm in modern hard disk drives. The oil will be assumed to be a constant viscosity, μ, incompressible Newtonian fluid. The bearing will be assumed to be concentric with the journal; this assumption means that the properties of the system are the same whether the grooves are on the inner or outer cylinders [10]. Both configurations have been considered in other studies [13], but having the grooves on the outer cylinder has been shown to have many important advantages.

In the simplest case, the herring-bone pattern will be considered to be diagonal grooves forming V's with a groove angle β and piecewise constant gap depth of $\tilde{h}_g$ in the grooves and $\tilde{h}_L$ in the land regions with $\tilde{h}_g > \tilde{h}_L$ (see Fig. 3 for a side view and a plan view of the bearing).

2.2 The governing equation

A dimensionless Reynolds number can be defined for this problem as $\mathrm{Re} = \tilde{\Omega}\tilde{R}\tilde{h}_L/\nu$. While $\tilde{\Omega}$ is large, so is the viscosity of the oil and the clearance is very small, so overall the Reynolds number is close to zero. Consequently the hydrodynamics of the oil, as described by the Stokes equation and for steady-state flow in a long narrow channel the behavior of the pressure $\tilde{p}(\tilde{x}, \tilde{z})$ will therefore be well-approximated by the steady-state Reynolds equation of lubrication theory [5, 6, 9],

$$\frac{\tilde{U}}{2}\frac{\partial \tilde{h}}{\partial \tilde{x}} = \frac{1}{12\tilde{\mu}}\tilde{\nabla}\cdot\left(\tilde{h}^3\nabla\tilde{p}\right) \tag{1}$$

where we have introduced the relative speed $\tilde{U} = \tilde{\Omega}\tilde{R}$. We seek the solution for the problem in the reference frame where the grooves are fixed and the smooth bearing slides by with speed $\tilde{U}$. The gap height function will generally assumed to be of the form

$$\tilde{h}(\tilde{x}, \tilde{z}) = \begin{cases} \tilde{h}_L & \text{in the land regions (between grooves),} \\ \tilde{h}_g & \text{in grooves.} \end{cases} \tag{2}$$

The problem for determining the pressure in the oil $\tilde{p}(\tilde{x}, \tilde{z})$ is then set by specifying the groove properties and boundary conditions on (1):

- There are N identical evenly-spaced grooves.
- BC: The domain is periodic in $\tilde{x}$, $\tilde{x} \in [0, 2\pi\tilde{R}]$.
- BC: The oil is open to ambient pressure, $\tilde{p} = p_{\text{atm}}$, at the top/bottom of the journal $\tilde{z} = \pm\tilde{H}$. (here p_{atm} is atmospheric pressure).
- BC: The grooves are symmetric about the line $\tilde{z} = 0$ so that the pressure must also have this even symmetry with respect to $\tilde{z}$, $\partial_{\tilde{z}}\tilde{p}(\tilde{x}, 0) = 0$.

2.3 The scaled problem

We nondimensionalize the problem using the scalings

$$\tilde{z} = \frac{2\pi\tilde{R}}{N} z, \qquad \tilde{x} = \frac{2\pi\tilde{R}}{N} x, \qquad \tilde{h} = \tilde{h}_L h, \qquad \tilde{p} = p_{\text{atm}} \left(1 + \frac{2\pi}{N}\Lambda p\right), \tag{3}$$

where the pressure scale is given in terms of the bearing number,

$$\Lambda = \frac{6\mu\tilde{\Omega}}{p_{\text{atm}}} \left(\frac{\tilde{R}}{\tilde{h}_L}\right)^2. \tag{4}$$

Then the dimensionless problem is

$$\nabla \cdot (h^3 \nabla p) = \frac{\partial h}{\partial x}, \tag{5a}$$

where, if $h(x, z)$ is specified, this is a generalized form of a Poisson problem for $p(x, z)$. To obtain the solution on the entire journal it is sufficient to solve it over one unit cell with $0 \le x \le 1$ and $0 \le z \le \Gamma$ with $\Gamma = N\tilde{H}/(2\pi\tilde{R})$, see Fig. 4. The scaled height is

$$h(x, z) = \begin{cases} 1 & \text{on land regions (between grooves),} \\ 1/\epsilon & \text{in grooves,} \end{cases} \tag{5b}$$

where we define the height ratio $\epsilon = \tilde{h}_L/\tilde{h}_g \le 1$. The boundary conditions on the unit cell are periodic in x, and Neumann in the mid-plane, and Dirichlet at the top:

$$p(0, z) = p(1, z), \qquad p_z(x, 0) = 0, \qquad p(x, \Gamma) = 0. \tag{5c}$$

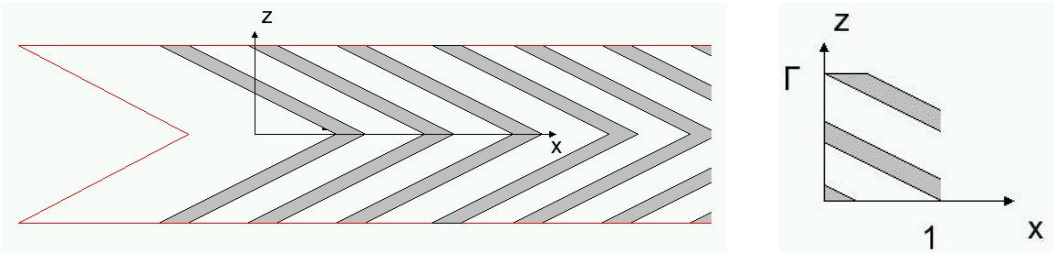

Figure 4: The unwrapped groove pattern (left) and the fundamental unit cell (right). The grooves are the shaded regions.

3 Design goals

Having derived the governing problem for the pressure $p(x, z)$ given a height $h(x, z)$ we now return to the problem of physical interest. The grooves are typically made to be of constant depth for manufacturing simplicity. There are however numerous different designs for the groove shapes. The simplest and most common is the V-shaped grooves shown in Fig. 4. Here we are interested in finding shapes for the grooves that will avoid the negative pressures that occur in such V-shaped designs. Hence one design aim is maximize the minimum pressure in the bearing. There is however, one simple case that does this and that is to have no grooves in the bearing, in which case, the solution is $p(x, z) \equiv 0$ and this is a very poor bearing as it has no stiffness so will result in the spindle wobbling. The main design aim that previous work has concentrated on is making the bearing very stiff and this is most readily expressed as seeking to maximize the load on the bearing. For our purposes the two aims, in nondimensional form are:

$$\text{Remove negative pressure:} \qquad \text{maximize}\Big(\min(p(x,z)\Big) \tag{6}$$

$$\text{Make the bearing stiff:} \qquad \text{maximize}\left(\iint p(x,z)dA\right) \tag{7}$$

Because the second aim seeks very high pressures it turns out that these two aims are in conflict with each other.

In the following sections we shall present work to consider various groove designs and to solve the forward problem in order to determine the minimum pressure and the load in each case. We shall also present different methods for seeking to find an optimal shape for the grooves based on some combination of the two design aims.

4 Numerical approaches

As the overall aim of the investigation is to optimize the groove shape a number of numerical approaches were considered. Having used these to solve the forward problem, where $h(x, z)$ is given, various investigations were then considered.

4.1 Finite difference approach for the forward problem

In order to solve the boundary-value problem defined by (5a), (5b) and (5c) , we first introduce a uniform grid covering the domain $0 \le x \le 1$ and $0 \le z \le \Gamma$. We set

$$x_i = i\Delta x, \qquad z_j = \left(j - \frac{1}{2}\right)\Delta z, \qquad \Delta x = \frac{1}{M}, \qquad \Delta z = \frac{\Gamma}{N - \frac{1}{2}}$$

and let $P_{i,j}$ approximate $p(x_i, z_j)$ on the grid for $i = 0, 1, \ldots, M$ and $j = 0, 1, \ldots, N$. (The z_0 and z_1 grid lines straddle the boundary at $z = 0$ to facilitate the application of the zero-flux boundary condition there as indicated below.) The left-hand-side of the PDE in (5a) is in divergence form representing a conservation of mass. This form is preserved in a discrete sense in the following second-order accurate difference approximation

$$\frac{1}{\Delta x}\left(\mathcal{F}_{i+1/2,j} - \mathcal{F}_{i-1/2,j}\right) + \frac{1}{\Delta z}\left(\mathcal{G}_{i,j+1/2} - \mathcal{G}_{i,j-1/2}\right) = \frac{\partial h}{\partial x}(x_i, z_j) \tag{8}$$

for $i = 1, 2, \ldots M$ and $j = 1, 2, \ldots N - 1$, where

$$\mathcal{F}_{i-1/2,j} = \frac{h^3(x_{i-1/2}, z_j)}{\Delta x}\left(P_{i,j} - P_{i-1,j}\right), \quad \mathcal{G}_{i,j-1/2} = \frac{h^3(x_i, z_{j-1/2})}{\Delta z}\left(P_{i,j} - P_{i,j-1}\right),$$
$$\mathcal{F}_{i+1/2,j} = \frac{h^3(x_{i+1/2}, z_j)}{\Delta x}\left(P_{i+1,j} - P_{i,j}\right), \quad \mathcal{G}_{i,j+1/2} = \frac{h^3(x_i, z_{j+1/2})}{\Delta z}\left(P_{i,j+1} - P_{i,j}\right).$$

The boundary conditions are taken to be

$$\left.\begin{aligned} P_{0,j} &= P_{M,j} \\ P_{M+1,j} &= P_{1,j} \end{aligned}\right\}, \quad j = 1, 2, \ldots, N-1, \qquad \text{(periodic sides at } x = 0 \text{ and } 1)$$
$$P_{i,0} = P_{i,1}, \qquad i = 0, 1, \ldots, M, \qquad \text{(zero mass flux at } z = 0)$$
$$P_{i,N} = 0, \qquad i = 0, 1, \ldots, M. \qquad \text{(ambient pressure at } z = \Gamma)$$

Assuming the gap height $h(x, z)$ is known, the finite difference equations in (8) along with the boundary conditions form a linear system of $(M+1)(N+1)$ equations for the values of $P_{i,j}$ on the grid. The linear system is sparse and may be solved using a number of available software packages. We used Matlab for relatively coarse grids and an iterative sparse matrix solver in Fortran for finer grids.

4.2 Numerical results for various groove shapes

The gap height $h(x, z)$ is specified by the pattern of grooves on the sleeve of the bearing. For our first series of numerical experiments, we consider a pattern with 10 equally spaced grooves on the sleeve. The centerline of a particular groove is chosen to be

$$G(z) = \frac{1}{2} - (\cot\alpha)z + \frac{\cot\beta - \cot\alpha}{\sigma} \ln\left[\frac{\cosh(\sigma(z - \Gamma))}{\cosh(\sigma\Gamma)}\right] \tag{9}$$

where α, β and σ are adjustable parameters. The first two parameters specify the inclination angles of the groove path at $z = \Gamma$ and $z = 0$, respectively, while σ determines the sharpness of the

transition from one angle to the other. The two plots in Figure 5 show the behavior of $G(z)$ for a range of values for α and σ with β fixed at 20°.

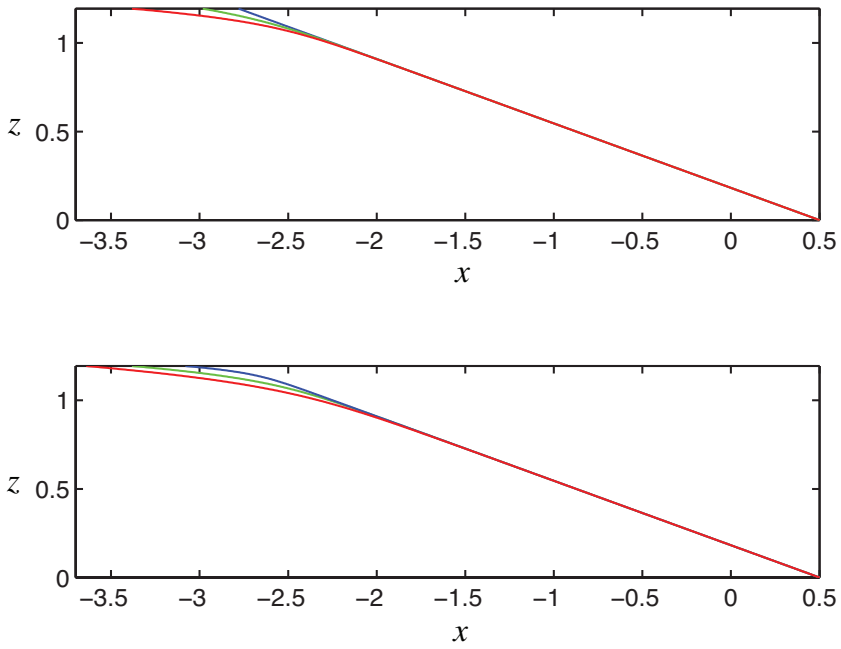

Figure 5: Groove paths for $\beta = 20°$: Top view is $\sigma = 10$ with $\alpha = 5°$ (red), 10° (green) and 20° (blue); Bottom view is $\alpha = 5°$ with $\sigma = 7$ (red), $\sigma = 10$ (green) and $\sigma = 20$ (blue).

Once the groove paths have been chosen, the gap height in the neighborhood of $G(z)$ is taken to be

$$h_G(x,z) = 1 - \frac{1}{2(1-1/\epsilon)}\left[\tanh(s(x - G(z) - \delta/2)) - \tanh(s(x - G(z) + \delta/2))\right]$$

where δ determines the width of the groove in the x-direction and s determines the sharpness of the transition from land at $h = 1$ to groove at $h = 1/\epsilon > 1$. In our calculations, we take $s = 200$ which gives a very sharp transition. The gap height behavior about the particular groove given by h_G is repeated periodically so that $h(x,z)$ is defined everywhere, including the computational domain $0 < x < 1$, $0 < z < \Gamma$. Figure 6 shows the behavior of $h(x,z)$ in the computational domain for a groove path with $\sigma = 10$, $\alpha = 5°$ and $\beta = 20°$, and for a groove width $\delta = 0.3$.

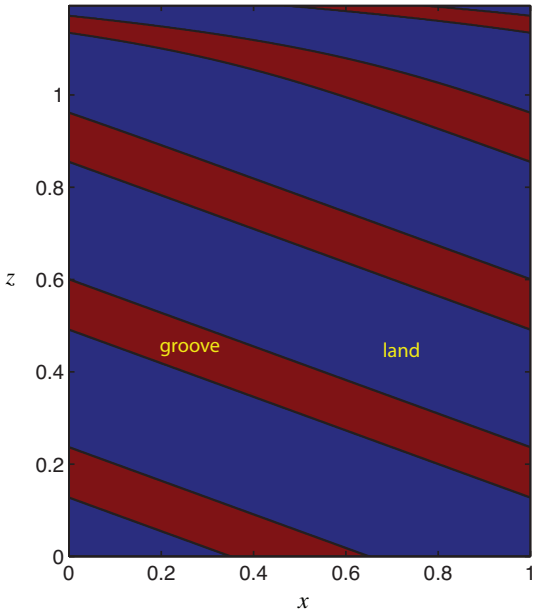

Figure 6: Gap height $h(x, z)$ for the groove path $G(z)$ with $\alpha = 5°$, $\beta = 20°$ and $\sigma = 10$, for the width $\delta = 0.3$.

As a first set of numerical experiments, we consider the behavior of the pressure for a range of choices of the parameters that specify the gap height $h(x, z)$. For each case, we compute the minimum pressure and the load in the oil bearing from the numerical solution using

$$P_{\min} = \min_{i,j} P_{i,j}, \qquad \text{and} \qquad F = \sum_{i=1}^{M} \sum_{j=1}^{N} P_{i,j} \Delta x \Delta z \; .$$

These two numerical quantities can then be used for the design goals (6) and (7) to assess the merit of the choice for the groove pattern. The idea is to determine general design trends which can then be used to guide optimization strategies to simultaneously maximize $P_{\min}$ and maximize F.

Figures 7 and 8 show the behavior of the load and the minimum pressure for straight grooves ($\sigma = 0$) with $\alpha = \beta = 20°$. Figure 7 shows the behavior as the width δ of the grooves is varied with depth parameter ϵ held fixed at $1/3$. As δ decreases, the load generated in the bearing decreases. This is due to the reduced mass of fluid pumped towards the center ($z = 0$) of the bearing as δ decreases. The minimum pressure is less than zero for all values of δ considered, and the magnitude of the minimum pressure decreases as δ decreases. As the design criteria seek large loads and minimum pressure, depending on the relative merit of these two items, there may be an optimal value of δ for fixed ϵ.

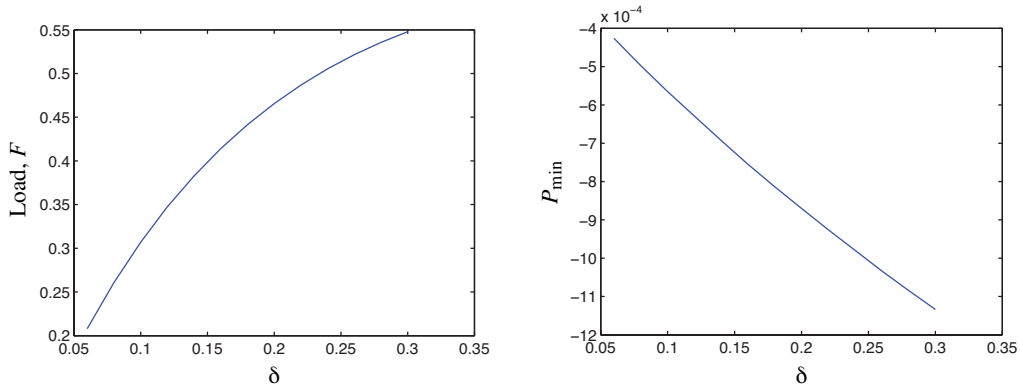

Figure 7: Load and minimum pressure versus groove width δ for straight grooves ($\sigma = 0$) with $\alpha = \beta = 20^\circ$ and $\epsilon = 1/3$.

Figure 8 shows the behavior of the load and the minimum pressure as the depth of the grooves varies with δ held fixed at 0.1. On one extreme when $\epsilon = 1$, the depth of the grooves is equal to that of the land so that $p = 0$ everywhere and thus the load and minimum pressure are both zero. As ϵ decreases from 1, the depth of the grooves increases and they act to pump increasing fluid mass towards the center of the bearing so that the load increases. The load continues to increase until a maximum is achieved near $\epsilon = 0.25$. For small values of ϵ at the other extreme, the depth of the grooves is very large relative to the land so that the pressure on the land is nearly zero, and the pump is less effective and generates a small load. The minimum pressure approaches zero near $\epsilon = 0$ and 1, and achieves a minimum near $\epsilon = 0.65$. It is clear that the trend for the minimum pressure, as ϵ varies, favors values closer to zero or close to unity, and if a high load is desired, then ϵ close to 0.25 would be ideal (for the chosen values for $\alpha = \beta$ and δ).

We next consider the behavior for the case $\sigma > 0$ when the grooves are "feathered" near $z = \Gamma$. Figure 9 shows the behavior of the load and minimum pressure for grooves with $\beta = 20^\circ$, $\sigma = 10$, $\delta = 0.3$ and $\epsilon = 1/3$ held fixed while α varies from 20° down to 2°. For values of α between 20° and 10°, approximately, the load remains fairly constant while the minimum pressure steadily increases. As α decreases from 10°, the load decreases but only slightly as compared to the range of values seen in the previous graphs. The minimum pressure, on the other hand, continues its increase until $\alpha = 2^\circ$ when it is very small, equal to -5×10^{-5} approximately. This trend shows promise and its appears that it is possible to design a groove path such that the load is above an acceptable value while the minimum pressure is nearly zero.

As an illustration of the solution for feathered grooves, Figure 10 shows the gap height $h(x, z)$ and the computed pressure $p(x, z)$ for grooves with $\alpha = 2^\circ$, $\beta = 20^\circ$, $\delta = 0.3$, $\epsilon = 1/3$ and $\sigma = 10$. The path of the grooves determined by $G(z)$ in (9) is inclined at $\beta = 20^\circ$ over most of the domain, but bends over to an angle $\alpha = 2^\circ$ at $z = \Gamma$. The gap width is constant so that the ratio of the total x-distance of groove to land is constant for any z. The pressure in the gap achieves a maximum at the trailing edge of the groove along the centerline, $z = 0$, and then generally decreases as z increases towards $z = \Gamma$. Following the grooves, the pressure increases nearly linearly from the centerline, while there is a near linear increase in the pressure vertically in the gap over the land.

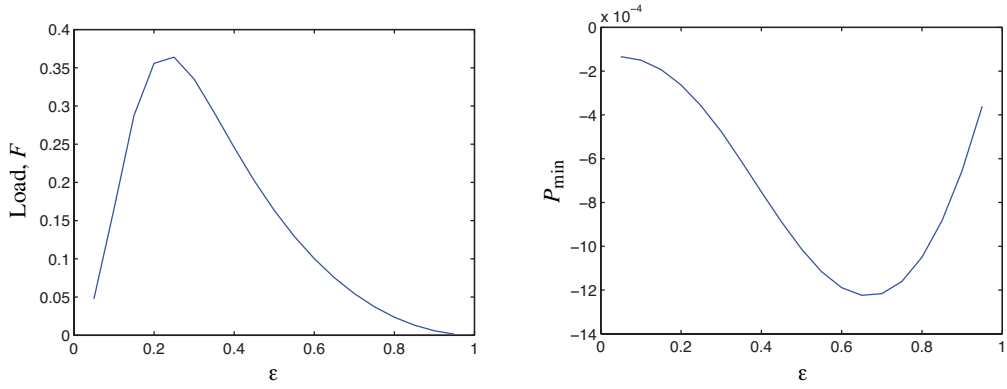

Figure 8: Load and minimum pressure versus groove depth parameter ϵ for straight grooves with $\alpha = \beta = 20°$ and $\delta = 0.1$. (The value for σ is not needed for straight grooves.)

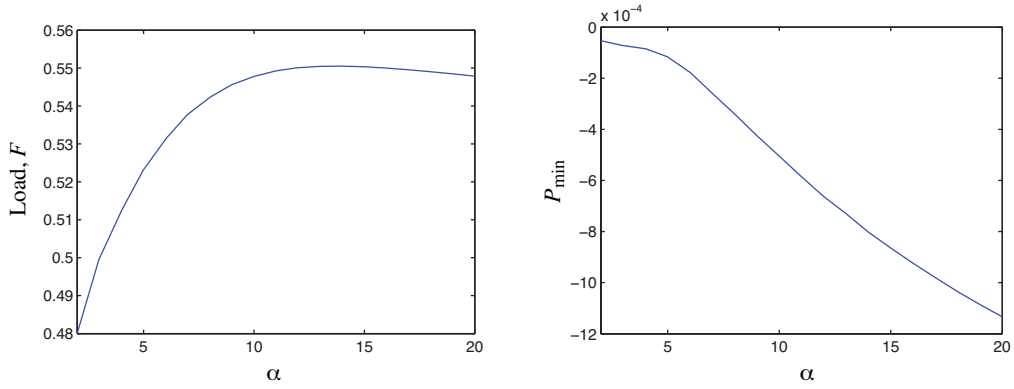

Figure 9: Load and minimum pressure versus groove angle α for feathered grooves with $\beta = 20°$, $\delta = 0.3$, $\epsilon = 1/3$ and $\sigma = 10$.

For z near Γ, the pressure flattens out to a value close to zero with only tiny pockets of negative pressure near the top of the view. Figure 11 shows a three-dimensional shaded contour of plot of pressure for the full gap. This plot is obtained from the pressure plot in Figure 10 using suitable periodic repetitions of the plots and an even reflection about $z = 0$.

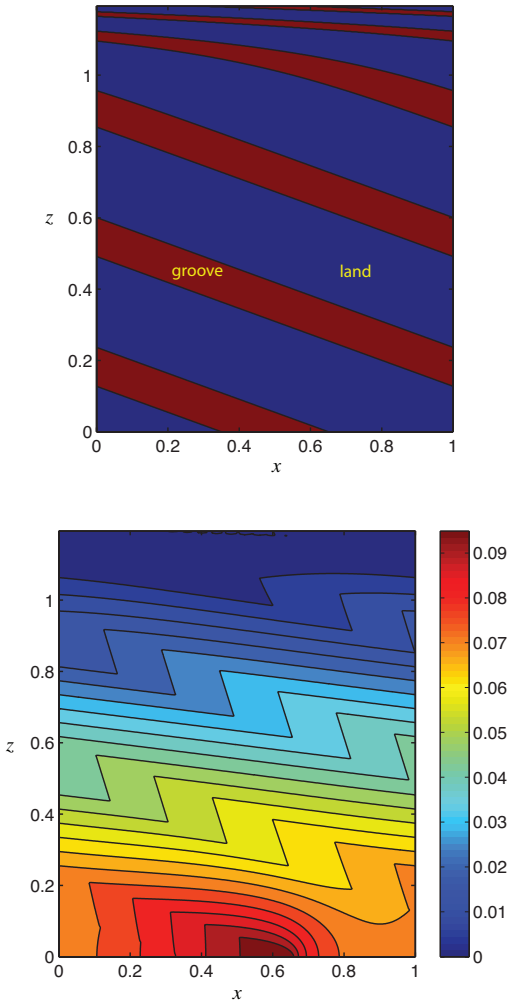

Figure 10: Shaded contours of the gap height (left) and the pressure (right) for feathered grooves with $\alpha = 2°$, $\beta = 20°$, $\delta = 0.3$, $\epsilon = 1/3$ and $\sigma = 10$.

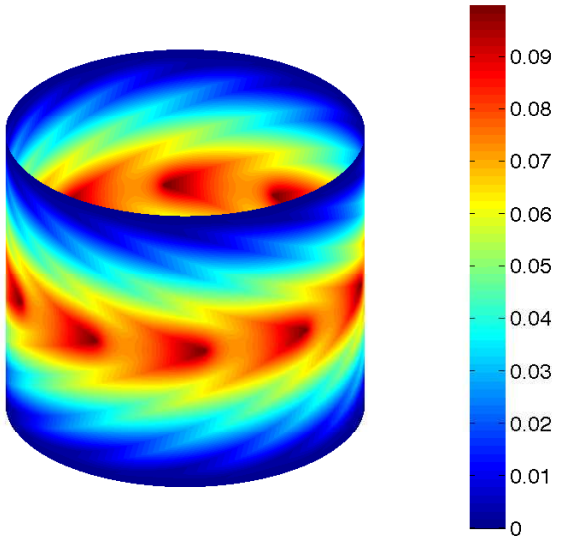

Figure 11: Shaded contours of pressure in the gap for feathered grooves with $\alpha = 2°$, $\beta = 20°$, $\delta = 0.3$, $\epsilon = 1/3$ and $\sigma = 10$.

4.3 Finite element solutions

The problem (5a), (5b) and (5c) was also considered numerically using the finite element package Femlab. The problem considered has straight grooves ($\sigma = 0$) and the solutions were found for various values of the groove angle β and bearing width Γ. The values used were chosen for simplicity of describing the region. The method used allows the thickness h to be described as a piecewise constant corresponding to $s \to \infty$. The results are summarized in table 1 with both the resulting minimum pressure P_{min} and the maximum pressure P_{max}. Typical pressure distributions are shown in figure 12 for two particular values of the parameters. In each case the minimum pressure can be clearly seen to occur at the boundary between the land and the groove at a short distance in from the bearing edge.

Γ	$\alpha = \beta$	P_{min}	P_{max}
1/10	5.71	- 0.000465	0.00464
1/8	7.125	- 0.000566	0.00687
1/6	9.46	- 0.000581	0.0110
1/3	18.435	- 0.001606	0.0296
1/2	26.565	- 0.003566	0.0467
2/3	33.69	- 0.005555	0.0604
5/6	39.806	- 0.007371	0.0708
1	45.00	- 0.008970	0.0785

Table 1: Minimum and maximum pressures predicted by finite element solutions for straight grooves ($\sigma = 0$), sharp jumps ($s \to \infty$), equal groove and land widths ($\delta = 0.5$) and $\epsilon = 1/2$

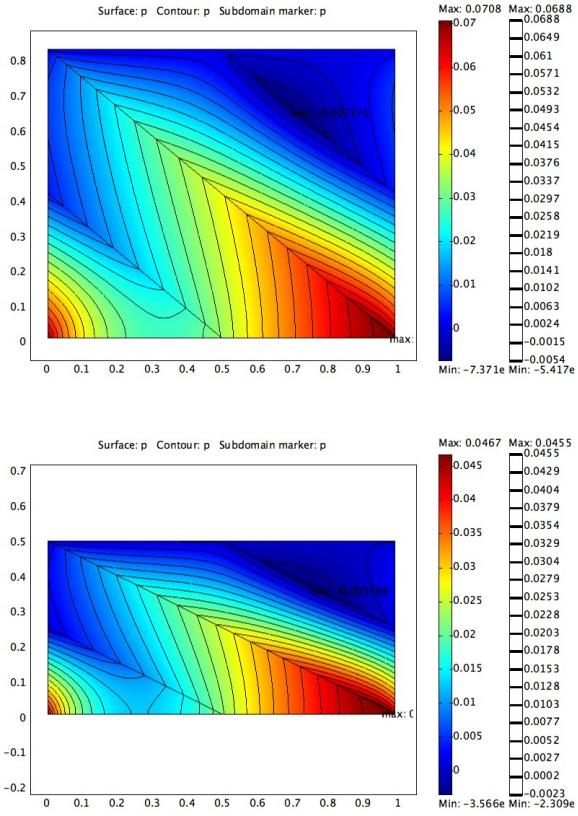

Figure 12: Shaded contours of pressure in the gap predicted by finite element solutions for straight grooves ($\sigma = 0$), sharp jumps ($s \to \infty$), equal groove and land widths ($\delta = 0.5$) and $\epsilon = 1/2$ (left has $\beta = 39.806$ $\Gamma = 5/6$, right has $\beta = 26.565$ $\Gamma = 1/2$

4.4 Optimization schemes

The finite difference scheme described earlier was used in a formal optimization procedure in order to gain insight into a possible optimal groove shape.

The multicanonical Monte Carlo method (mmc), developed in the area of statistical physics by Berg [3], is an iterative tool used to calculate meaningful statistics about rare events. In particular, the method has been implemented to explore the tail of probability distributions whose values are on the order of a once-in-the-age-of-the-universe event [7]. Here we wish to conduct numerical experiments using the multicanonical Monte Carlo method to find land/groove patterns that maximize the minimum pressure and load.

We consider representing the land/groove pattern as simply a matrix $H \in \mathbf{R}^{m\times n}$ with each component taking on the value 1 or $1/\epsilon$ and representing the evaluation of $h(x,z)$ at the necessary grid points for numerical calculations. The collection of all possible matrices H of this form is called the state space Ω and contains 2^{nm} elements. One way to systematically choose matrices from the space Ω is to draw them according to the uniform distribution, $\pi(H) = 2^{-nm}$. Once a land/groove pattern or the matrix H is chosen, the pressure can be calculated numerically as described above.

In order to allow the optimization procedure to be automated it is necessary to put the two design criteria ((6) and (7)) into a single objective function. The precise nature of this should depend on the relative merits of the two aspects but for the purpose of demonstrating the technique the the objective function

$$J(p) = \alpha_1 \frac{1}{\iint p \; dA} - \alpha_2 \; p_{\min} \; ,$$

where $p_{\min} = \min\left(p(x,z)\right)$ and the constants, α_1 and α_2, weight the relative importance of the two criteria with $\alpha_1 + \alpha_2 = 1$ and $\alpha_1, \alpha_2 \geq 0$. Hence for any $h(x,z)$ we can calculate J and the goal is to find the $h(x,z)$ that minimizes J.

Both H and J are random variables and the multicanonical Monte Carlo method will allow us to reconstruct the discretized probability density function (pdf) for J. The reconstruction will uncover land/groove patterns H with minimum values of J.

The pdf for J is discretized by dividing the range of J into B bins, $J_0 < J_1 < ... < J_B$, and letting P_b denote the probability that J lands in bin b when H is drawn according to $\pi(H)$. Recall, from probability theory, that P_b is equal to the expected value of the indicator function for the event when J lands in bin b with H is drawn according to $\pi(H)$. That is,

$$P_b = E\left[\chi_b\right], \qquad b = 1, ..., B,$$

where χ_b is the indicator function

$$\chi_b = \begin{cases} 1, & \text{if } x \in \Omega_b \\ 0, & \text{otherwise} \end{cases}$$

and $\Omega_b = \{H \in \Omega : J_{b-1} < J(p(H)) < J_b\}$. Notice, $\sum P_b = 1$.

One way to estimate the P_b's is with the Monte Carlo method. In the Monte Carlo method, the estimate p_b for P_b is defined as

$$p_b = \frac{1}{R} \sum_{j=1}^{R} \chi_b \left(H^{(j)}\right),$$

where $H^{(1)}, ..., H^{(R)}$ is an R-sample drawn according to $\pi(H)$. It can be shown that the uncertainty in the estimates p_b's decreases like $R^{-1/2}$. Moreover, if $P_b << 1$ then R must be on the order of

P_b^{-1} for the method to capture the statistic. Therefore, success is dependent upon the bin number b. In particular, as shown in Figure 13, it is troublesome to reconstruct the pdf for small positive values of J since the bins are hardly visited.

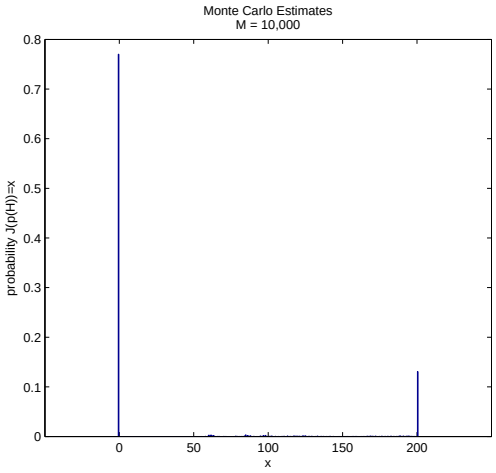

Figure 13: Monte Carlo estimates for J with $\alpha_1 = .6$ and $\alpha_2 = .4$. Small positive values are not captured by this simulation.

The idea behind the multicanonical Monte Carlo method is to draw the R-sample from a weighted distribution

$$\hat{\pi}(H) = \frac{\pi(H)}{w(H)}, \qquad w(H) = \sum_{b=1}^{B} \frac{\chi_b(H)}{w_b},$$

where the positive constants, $w_1, ..., w_B$, are chosen such that each bin is visited equally. Therefore, we wish to pick the w_b's so that the average number of times we land in bin b

$$E[\chi_b] = P_b w_b,$$

when H is drawn according to $\hat{\pi}(H)$, is independent of the bin number b. This equi-distributed case can be achieved by letting

$$P_b w_b = 1/B,$$

where $1/B$ comes from the requirement that the integral of the weighted distribution $\hat{\pi}(H)$ over the state space Ω must equal 1. That is, $\sum P_b w_b = 1$. Of course, there is one glaring problem with choosing the weights to be $w_b = (P_b B)^{-1}$. The P_b's are unknown! To get around this we set up an iteration. Basically we start with Monte Carlo sampling, pause to analyze the histogram, adjust the weights to heavily favor underrepresented bins, and iterate. The adjustment is called Berg's iteration [3, 12]. In practice, the Monte Carlo sampling is done using a Markov chain Monte Carlo routine. Further details can be found in [7].

In the forward pressure problem, the unit periodic cell domain $[0, 1] \times [0, \Gamma]$ is discretized with N horizontal and M vertical nodes. The number of evaluations of h essential to numerically solve the Reynolds' equation equals $(2M - 1)(N - 1)$ and are marked by x's in Figure 14. We chose to

format the matrix $H \in \mathbf{R}^{(2M-1)\times(N-1)}$ in the following manner $H(i,j) = h_{j+\mathrm{mod}(i+1,2)/2,i/2}$ where $h_{i,j} = h(x_i, z_j)$, $x_i = (i-1)\Delta x$ and $z_j = (j-1)\Delta z$.

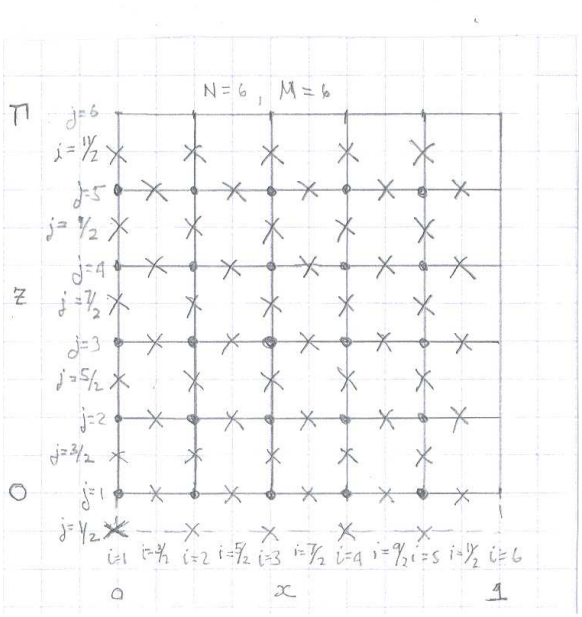

Figure 14: The computational domain of the forward problem with x's representing the grid evaluations of h needed for computation. The matrix H contains these h values.

The multicanonical Monte Carlo (mmc) method was run for 10 iterations on a computational domain constructed with $N = M = 50$. The parameters α_1 and α_2 were selected to be .6 and .4 respectively placing slightly more emphasis on maximizing the load as oppose to the minimum pressure. The largest value of minimum pressure encountered during the entire simulation was $p_{\min} = -.0022$ with load $= .0109$. Figure 15 displays the land/groove pattern producing this largest minimum pressure with the dots representing the groove.

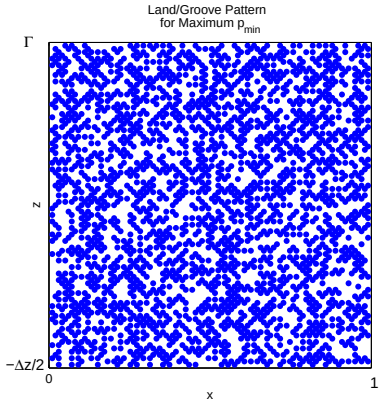

Figure 15: The land/groove pattern corresponding to the largest value of the $p_{\min}$ found. The dots represent the groove.

On the other hand, the smallest value of J encountered was 43.3203 with $p_{\min} = -.0033$ and load = .0139. The land/groove pattern is shown in Figure 16 and appears to be quite random. Further examination of these needs to be done.

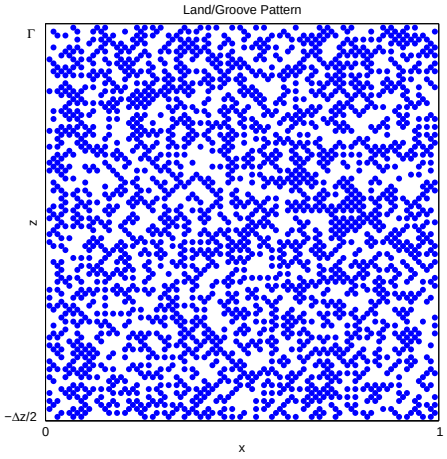

Figure 16: The land/groove pattern corresponding to the smallest value of the J found. The dots represent the groove.

The mmc method does create a ratchet effect that keeps any matrix H that drifts into a bin that appears to be less likely to be visited. That is, the bins associated with small positive values of J. The downfall in this method lies in the keyword "drifts". A better approach to finding the optimal matrix H that minimizes the objective function J would be a steepest descent approach.

The results presented here are indicative of the outcomes that can be generated from this method. A number of different enhancements to the procedure could be pursued with the hope

that these would generate physically more acceptable solutions for the optimal $h(x,z)$. These include, searching a state space of H that is much coarse that the resolution of the numerical scheme so that the pressure is more fully resolved and using a type of "multi-grid" method to search for optimal $h(x,z)$ on a very coarse mesh before refining the search to a finer mesh. These ideas remain to be explored but fit into the general strategy outline here.

5 Analysis

The next section considers some ideas based on an analytical approach with the aim of determining the behavior of the pressure distribution near the outer boundary of the bearing and hence the region where the minimum pressure occurs.

5.1 Piecewise constant height problem

It is convenient to re-write (5a) in terms of a mass flux vector,

$$\mathbf{q} = h^3 \nabla p - h\,\mathbf{i}\,, \qquad \nabla \cdot \mathbf{q} = 0, \tag{10}$$

where $\mathbf{i}$ is the unit vector in the x-direction. In regions where h is constant, the flux is proportional to the gradient of the pressure and the Reynolds equation reduces to Laplace's equation for the pressure,

$$\nabla^2 p = 0. \tag{11a}$$

At the boundaries between grooves and land, the pressure must be continuous

$$p(g(z)_-, z) = p(g(z)_+, z), \tag{11b}$$

(where $x = g(z)$ is taken as the land/groove boundary) and to conserve mass, the normal component of the flux must also be continuous, $(\mathbf{q}\cdot\mathbf{n})_- = (\mathbf{q}\cdot\mathbf{n})_+$, or written out in-full,

$$\left(h^3 p_{xx} - h - g'(z) h^3 p_{oz}\right)_- = \left(h^3 p_{xx} - h - g'(z) h^3 p_{zz}\right)_+, \tag{11c}$$

where $\mathbf{n} = (\mathbf{i} - g'(z)\,\mathbf{k})/\sqrt{1+g'(z)^2}$ and h changes from $h = 1$ to $h = 1/\epsilon$ across the boundary. Additionally, the homogeneous Dirichlet and Neumann conditions at $z = \Gamma$ and $z = 0$ are still needed. It is interesting to note that since the pressure satisfies Laplace's equation (11a) on each land or groove region it is a piecewise harmonic function. Harmonic functions cannot have interior local maxima or minima. Consequently it must be the case that any local minimum of the pressure will occur on a land/groove boundary. The maximum is expected to occur on the $z = 0$ midplane from physical considerations. If there is no pressure minimum along the land/groove boundaries then the minimum pressure is $p = 0$ (imposed by the $z = \Gamma$ Dirichlet boundary condition).

5.2 Local analysis at a land/groove boundary

Consider a polar coordinate system shifted to be centered at the $z = \Gamma$ endpoint of a land/groove boundary, see Fig. 17. Laplace's equation in polar coordinates is given by

$$\frac{1}{r}\frac{\partial}{\partial r}\left(r\frac{\partial p}{\partial r}\right) + \frac{1}{r^2}\frac{\partial^2 p}{\partial \theta^2} = 0, \tag{12}$$

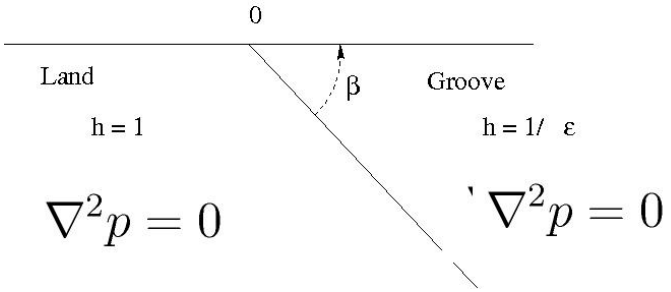

Figure 17: The problem for local analysis at the top edge of a groove/land interface.

with general solution of the form

$$p(r,\theta) = \sum_{\lambda} c_\lambda r^\lambda e^{i\lambda\theta}. \tag{13}$$

We now solve for the coupled pressures in the land, p_L, and the groove, p_g. Both have Dirichlet condition $p = 0$ imposed on the horizontal axis, hence

$$p_g(r,\theta) = \sum_{\lambda} a_\lambda r^\lambda \sin[\lambda\theta], \qquad -\beta \le \theta \le 0 \tag{14a}$$

$$p_L(r,\theta) = \sum_{\lambda} b_\lambda r^\lambda \sin[\lambda(\theta-\pi)], \qquad \pi \le \theta \le 2\pi - \beta, \tag{14b}$$

On the boundary, the pressure must be continuous, and at each order in $O(r^\lambda)$ we obtain the relation:

$$b_\lambda \sin[\lambda(\beta+\pi)] = a_\lambda \sin[\lambda\beta]. \tag{15}$$

In polar coordinates for the interface $z - \Gamma = -x\tan\beta$, the flux condition becomes

$$\sin\beta - \frac{1}{r}\frac{\partial p_L}{\partial\theta} = \frac{\sin\beta}{\epsilon} - \frac{1}{\epsilon^3}\frac{1}{r}\frac{\partial p_g}{\partial\theta} \qquad \text{at } \theta = -\beta. \tag{16}$$

Plugging the expansions (14a) and (14b) into this we obtain

$$\sin\beta - \sum \lambda b_\lambda r^{\lambda-1}\cos[\lambda(\beta+\pi)] = \frac{\sin\beta}{\epsilon} - \frac{1}{\epsilon^3}\sum \lambda a_\lambda r^{\lambda-1}\cos[\lambda\beta] \tag{17}$$

In order to balance the $O(r^0)$ terms in (17) we either need $\epsilon = 1$ (i.e. no groove – both regions are land), or one eigenvalue to be $\lambda = 1$:

$$\sin\beta - b_1\cos[\beta+\pi] = \frac{\sin\beta}{\epsilon} - \frac{a_1}{\epsilon^3}\cos[\beta]. \tag{18}$$

Moreover, from (15) with $\lambda = 1$, we obtain $a_1 = -b_1$, hence we determine that

$$a_1(\beta,\epsilon) = \frac{\epsilon^2\tan\beta}{1+\epsilon+\epsilon^2}. \tag{19}$$

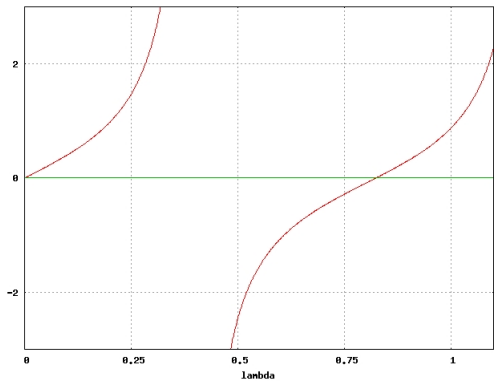

Figure 18: Roots of the function $F(\lambda)$, from (23), determine the eigenvalues.

This in fact defines a particular solution of the form

$$p_1(z) = a_1(\beta, \epsilon)(z - \Gamma). \tag{20}$$

This solution holds over both the land and the groove and describes linear growth of the pressure in z. It is somewhat unexpected that this solution is smooth across the boundary, but clearly shows that the pressure is generated by the groove depth and angle. This linear pressure cannot satisfy the condition as $z \to 0$ and hence the other terms in the expansion must be considered.

Returning to the $O(r^{\lambda-1})$ terms in the expansion, for $\lambda \neq 1$, we must have

$$b_\lambda \cos[\lambda(\beta + \pi)] = \frac{a_\lambda}{\epsilon^3} \cos[\lambda\beta]. \tag{21}$$

Equations (15, 21) form a linear homogeneous system of equations for unknown coefficients a_λ, b_λ:

$$\begin{pmatrix} \sin[\lambda\beta] & -\sin[\lambda(\beta+\pi)] \\ \cos[\lambda\beta] & -\epsilon^3 \cos[\lambda(\beta+\pi)] \end{pmatrix} \begin{pmatrix} a_\lambda \\ b_\lambda \end{pmatrix} = \begin{pmatrix} 0 \\ 0 \end{pmatrix}. \tag{22}$$

In order for nontrivial solutions to exist, the matrix must be singular (determinant equals zero), this condition yields a transcendental equation for the eigenvalues:

$$F(\lambda) = \tan[\lambda(\beta + \pi)] - \epsilon^3 \tan[\lambda\beta] = 0 \tag{23}$$

There is always a trivial solution for $\lambda = 0$, and from numerical calculations, see Fig. 18, we see there is always a positive eigenvalue with $\lambda_1 \leq 1$, having $\lambda_1 \to 1 - \beta(1 - \epsilon^3)/\pi$ as $\beta \to 0$. The case $\lambda_1 = 1$ only occurs in the physically unrealistic case of $\beta = 0$ and hence this eigenmode will, in practice, be sublinear. If we now consider the behavior of the pressure as we approach $z = \Gamma$ the solution (14a) and (14b) will be dominated by the eigenmode related to λ_1. We believe that this eigenmode creates the minimum pressure region near the bearing boundary. Attempts to quantify the dependency of the coefficients a_1 and b_1 on β to understand the behavior of this minimum have so far been unsuccessful.

6 Conclusions

The problem of determining the pressure distribution within a grooved bearing have been considered. Some insight has been gained using analysis indicating that a negative pressure will always exist when there are grooves and some indication of the position of the minimum pressure. Numerical methods have been exploited in order to solve the forward problem for the pressure when the groove geometry is known. Using the numerical methods the trends in the minimum pressure and in the total load as a function of some basic geometry of the grooves has been explored. In addition formal optimization methods have been used to find optimal designs when the two basics aims of the design in a single objective function. This work has therefore provided the basis for determining groove designs that remain very stiff, as in conventional designs but which also have only very small sub-atmospheric pressures.

7 Appendix

MATLAB code:
pres.m

```
%  Calculate pressure from matrix H
function Z = pres(H)


% Number of nodes N - horizontal and M - vertical
N = 50;
M = 50;

L = 1;
Height = (1.5*15)/(2*2*pi);

dx = L/(N-1);
dz = Height/(M-1);


% Build diff matrix along with rhs

D = zeros((N-1)*M,(N-1)*M);
b = zeros((N-1)*M,1);


for j=1:M
    if j==1
        for i=1:N-1
            if i==1
                d1= (H(2*j+1,i))^3 / (dz^2);
                d2=(H(2*j,N-1))^3 / (dx^2);
```

```
            d4=(H(2*j,i))^3 / (dx^2);
            d5= (H(2*j-1,i))^3/ (dz^2);

            d3 = -(d4+d2+d1+d5);
            D(nodeIndex(N,i,j),nodeIndex(N,i,j+1))=d1+d5;
            D(nodeIndex(N,i,j),nodeIndex(N,N-1,j))=d2;
            D(nodeIndex(N,i,j),nodeIndex(N,i,j))=d3;
            D(nodeIndex(N,i,j),nodeIndex(N,i+1,j))=d4;

            b(nodeIndex(N,i,j))= ( H(2*j,i) - H(2*j,N-1) ) / (dx);

        elseif i==N-1
            d1= (H(2*j+1,i))^3 / (dz^2);
            d2=(H(2*j,i-1))^3 / (dx^2);

            d4=(H(2*j,i))^3 / (dx^2);
            d5= (H(2*j-1,i))^3/ (dz^2);

            d3 = -(d4+d2+d1+d5);
            D(nodeIndex(N,i,j),nodeIndex(N,i,j+1))=d1+d5;
            D(nodeIndex(N,i,j),nodeIndex(N,i-1,j))=d2;
            D(nodeIndex(N,i,j),nodeIndex(N,i,j))=d3;
            D(nodeIndex(N,i,j),nodeIndex(N,1,j))=d4;

            b(nodeIndex(N,i,j))= ( H(2*j,i) - H(2*j,i-1) ) / (dx);
        else
            d1= (H(2*j+1,i))^3 / (dz^2);
            d2=(H(2*j,i-1))^3 / (dx^2);

            d4=(H(2*j,i))^3 / (dx^2);
            d5= (H(2*j-1,i))^3/ (dz^2);

            d3 = -(d4+d2+d1+d5);
            D(nodeIndex(N,i,j),nodeIndex(N,i,j+1))=d1+d5;
            D(nodeIndex(N,i,j),nodeIndex(N,i-1,j))=d2;
            D(nodeIndex(N,i,j),nodeIndex(N,i,j))=d3;
            D(nodeIndex(N,i,j),nodeIndex(N,i+1,j))=d4;


            b(nodeIndex(N,i,j))= ( H(2*j,i) - H(2*j,i-1) ) / (dx);
        end
    end
elseif j==M
    for i=1:N-1
        D(nodeIndex(N,i,j),nodeIndex(N,i,j))=1;
    end
```

```
else
    for i=1:N-1
        if i==1
            d1= (H(2*j+1,i))^3 / (dz^2);
            d2=(H(2*j,N-1))^3 / (dx^2);

            d4=(H(2*j,i))^3 / (dx^2);
            d5= (H(2*j-1,i))^3/ (dz^2);

            d3 = -(d4+d2+d1+d5);
            D(nodeIndex(N,i,j),nodeIndex(N,i,j+1))=d1;
            D(nodeIndex(N,i,j),nodeIndex(N,N-1,j))=d2;
            D(nodeIndex(N,i,j),nodeIndex(N,i,j))=d3;
            D(nodeIndex(N,i,j),nodeIndex(N,i+1,j))=d4;
            D(nodeIndex(N,i,j),nodeIndex(N,i,j-1))=d5;

            b(nodeIndex(N,i,j))= ( H(2*j,i) - H(2*j,N-1) ) / (dx);
        elseif i==N-1
            d1= (H(2*j+1,i))^3 / (dz^2);
            d2=(H(2*j,i-1))^3 / (dx^2);

            d4=(H(2*j,i))^3 / (dx^2);
            d5= (H(2*j-1,i))^3/ (dz^2);

            d3 = -(d4+d2+d1+d5);
            D(nodeIndex(N,i,j),nodeIndex(N,i,j+1))=d1;
            D(nodeIndex(N,i,j),nodeIndex(N,i-1,j))=d2;
            D(nodeIndex(N,i,j),nodeIndex(N,i,j))=d3;
            D(nodeIndex(N,i,j),nodeIndex(N,1,j))=d4;
            D(nodeIndex(N,i,j),nodeIndex(N,i,j-1))=d5;

            b(nodeIndex(N,i,j))= ( H(2*j,i) - H(2*j,i-1) ) / (dx);
        else
            d1= (H(2*j+1,i))^3 / (dz^2);
            d2=(H(2*j,i-1))^3 / (dx^2);

            d4=(H(2*j,i))^3 / (dx^2);
            d5= (H(2*j-1,i))^3/ (dz^2);

            d3 = -(d4+d2+d1+d5);
            D(nodeIndex(N,i,j),nodeIndex(N,i,j+1))=d1;
            D(nodeIndex(N,i,j),nodeIndex(N,i-1,j))=d2;
            D(nodeIndex(N,i,j),nodeIndex(N,i,j))=d3;
            D(nodeIndex(N,i,j),nodeIndex(N,i+1,j))=d4;
            D(nodeIndex(N,i,j),nodeIndex(N,i,j-1))=d5;
```

```
                b(nodeIndex(N,i,j))= ( H(2*j,i) - H(2*j,i-1) ) / (dx);
            end
        end
    end
end

    % Solve
D = sparse(D);
solution=D\b;
Z=reshape(solution,N-1,M);
Z=Z';

end
```

nodeIndex.m

```
function r=nodeIndex(N,i,j)
    r=(N-1)*(j-1)+i;
end
```

mmcdriver.m

```
function [hits,P,Pnew,Hsave,Accept,varsave,Hpmin, pmin] = mmcdriver( )
%  Multicanonical Monte Carlo

function [hits,Pc,Pnew,Hsave,Accept,varsave,Hpmin, pmin] = mmcdriverv3(H)
%  Multicanonical Monte Carlo

N = 50;                                          % no of columns in the matrix H
M = 50;                                          % no of rows in the matrix H

L = 1;
Height = (1.5*15)/(4*pi);
dx = L/(N-1);
dz = Height/(M-1);

binedge = -.5:1:200.5;                             % edges of target bins
binedge = [-2e10 binedge 2e10];
Nbin = length(binedge)-1;                        % no of bins
lenMCMC = 1e4;                                   % length of MCMC chaincode
burnin = 1e2;                                    % burn-in period for chains
Niter = 6;                                      % MMC iterations
epsilon = 1/3;

% ******************** Initialization ***************************

randn('state',sum(100*clock)), rand('state',sum(100*clock));
```

```
load Run3.mat
Pc = ones(Nbin,Niter)/Nbin;
Pc(:,1) = P(:,5);

hits = zeros(Nbin,Niter);
g = zeros(Nbin-1,Niter);
ghat = zeros(Nbin-1,Niter);
Pnew = zeros(Nbin,1);
Accept = zeros(Niter,1);

X = rand(2*M-1,N-1);
H = double(X>.5) + double(X<=.5)*(1/epsilon);
Hsave = cell(Niter,1);
varsave = cell(Niter,1);
Hpmin = cell(Niter,1);
pmin = cell(Niter,1);
alpha1 = .6;
alpha2 = .4;


for i = 1:Niter

    acceptval = randn(1,lenMCMC+burnin);
    index = ceil((N-1)*(2*M-1)*rand(1,lenMCMC+burnin));

    %  Calculate minimun pressure
    p = pres(H);
    minp = min(min(p));
    p(1,:) = .5*p(1,:);
    sump = sum(sum(p))*dx*dz;
    var = alpha1*(1/sump) - alpha2*(minp);
    Hsave{i} = {H};
    Hpmin{i} = H;
    varsave{i} = {var};
    pmin{i} = minp;
    [junk,bin] = histc(var,binedge);

    for m = 1:lenMCMC+burnin
        Hpro = H;
        row = ceil(index(m)/(N-1));
        col = (N-1) - mod(index(m),(N-1));
        if Hpro(row,col)==1
            Hpro(row,col) = 1/epsilon;
        else
            Hpro(row,col) = 1;
        end
```

```
    ppro = pres(Hpro);
    minppro = min(min(ppro));
    ppro(1,:) = .5*ppro(1,:);
    sumppro = sum(sum(ppro))*dx*dz;
    varpro = alpha1*(1/sumppro) - alpha2*minppro;
    [junk,newbin] = histc(varpro,binedge);

    %  Accept proposal?
    alpha = min(1,Pc(bin,i)/Pc(newbin,i));
    if acceptval(m) < alpha
        H = Hpro;  bin = newbin; var = varpro; minp = minppro;
        if m>burnin
            Accept(i) = Accept(i) + 1;
        end
        if pmin{i} < minp
            Hpmin{i} = H;
            pmin{i} = minp;
        end

        if bin>=2 && bin<=50
            Hsave{i} = {Hsave{i}{1:end}, H};
            varsave{i} = {varsave{i}{1:end}, var};
        end

    end

    if m>burnin
        hits(bin,i) = hits(bin,i) + 1;
    end

end

%  Berg update.

Pnew = Pc(:,i);
for k=1:(Nbin-1)
    if (hits(k+1,i)*hits(k,i)>0)
        g(k,i) = hits(k+1,i)*hits(k,i)/(hits(k+1,i)+hits(k,i));
        ghat(k) = g(k,i)/(sum(g(k,1:i)));
        Pnew(k+1) = Pnew(k)*(Pc(k+1,i)/Pc(k,i))*((hits(k+1,i)/hits(k,i))^ghat(k));
    else
        Pnew(k+1) = Pnew(k)*(Pc(k+1,i)/Pc(k,i));
    end
end

Pc(:,i) = Pnew/sum(Pnew);
```

```
save Run5.mat Pnew Pc hits Accept varsave Hsave Hpmin pmin binedge
end
end
```

References

[1] T. Asada, H. Saito, Y. Asaida, and K. Itoh. Characteristic analysis of hydrodynamic bearings for HDDs. *IEEE Transactions on Magnetics*, 37(2):810–814, 2001.

[2] T. Asada, H. Saito, Y. Asaida, and K. Itoh. Design of hydrodynamic bearings for high-speed HDD. *Microsystem Technologies*, 8:220–226, 2002.

[3] B. A. Berg. Introduction to multicanonical Monte Carlo simulations. *Fields Institute Communications*, 26:1–24, 2000.

[4] D. Bonneau and J. Absi. Analysis of aerodynamic journal bearings with small number of herringbone grooves by finite element method. *Journal of Tribology*, 116:698–704, 1994.

[5] A. Cameron. *The principles of lubrication*. Longmans, London, 1966.

[6] V. N. Constantinescu. *Laminar viscous flow*. Springer Verlag, New York, 1995.

[7] T. Driscoll and K. Maki. Searching for rare growth factors using multicanonical Monte Carlo methods. *SIAM Revier*, To appear.

[8] A. M. Gad, M. M. Nemat-Alla, A. A. Khalil, and A. M. Nasr. On the optimum groove geometry for herringbone grooved journal bearings. *Journal of Tribology*, 128:585–593, 2006.

[9] B. J. Hamrock. *Fundamentals of fluid film lubrication*. McGraw-Hill, New York, 1994.

[10] F. Hendriks. Thousand-fold oil-air interface scale-up in fluid dynamic bearings of hard disk drives. *IEEE Transactions on Magnetics*, 42(10):2597–2599, 2006.

[11] F. Hendriks, B. S. Tilley, J. Billingham, P. J. Dellar, and R. Hinch. Dynamics of the oil-air interface in hard disk drive bearings. *IEEE Transactions on Magnetics*, 41(10):2884–2886, 2005.

[12] R. Holzlöhner and C. R. Menyuk. Use of multicanonical Monte Carlo simulations to obtain accuracte bit error rates in optical communications systems. *Optics Letters*, 28(20):1894–1896, 2003.

[13] G. H. Jang and J. W. Yoon. Nonlinear dynamic analysis of a hydrodynamic journal bearing considering the effect of a rotating or stationary herringbone groove. *Journal of Tribology*, 124:297–304, 2002.

[14] G. H. Jang and J. W. Yoon. Stability analysis of a hydrodynamic journal bearing with rotating herringbone grooves. *Journal of Tribology*, 125:291–300, 2003.

[15] T. S. Lee, Y. G. Liu, and S. H. Winoto. Analysis of liquid-lubricated herringbone grooved journal bearings. *International Journal of Numerical Methods for Heat and Fluid Flow*, 14(3):341–365, 2004.

[16] T. V. V. L. N. Rao and J. T. Sawicki. Stability characteristics of herringbone grooved journal bearings incorporating cavitation effects. *Journal of Tribology*, 126:281–287, 2004.

[17] C. C. Rondonuwu and S. H. Winoto. Pressure distributions along vertical hydrodynamic herringbone-grooved journal bearings. *Tribology Transactions*, 49:174–181, 2006.

[18] N. Zirkelback and L. San Andres. Finite element analysis of herringbone groove journal bearings: a parametric study. *Journal of Tribology*, 120:234–240, 1998.